

Configurable AC electroosmotic generated in-plane microvortices and pumping flow in microchannels

Shih-Hao Huang · Hui-Jung Hsueh ·
Kuo-Yung Hung

Received: 11 March 2009 / Accepted: 20 April 2009 / Published online: 14 May 2009
© Springer-Verlag 2009

Abstract This paper proposes the patterned AC electroosmotic flows (AC-EOF) by simply grouping discrete electrodes together to form various electrode configurations for generation of in-plane microvortices with clockwise/counter-clockwise rotation, and pumping flow in a microchannel. The rotational direction of in-plane microvortices and pumping flow direction can be controlled using the same electrode pattern by simple switching of the voltages on the electrodes. Microparticle image velocimetry (μ PIV) was used to characterize the flow fields of the generated in-plane microvortices and pumping flow. The rotational strength of microvortices and flow rates of pumping flows were found to increase with the increase of the applied voltages, and an optimal value was achieved at an appropriately applied frequency. Moreover, the dependency of the applied voltages, frequencies, and the heights of the measured planes on the rotational strength of in-plane microvortices between the interdigitated and discrete electrode configurations were examined. The discrepancy in electrode geometry results in a small performance reduction, whereas it can be compensated for the ability of switching the rotational direction of in-plane microvortices using the same device. The configurable in-plane microvortices and pumping flow in microchannels provide the

potential for micromixing applications and for the integration into a lab-on-a-chip system.

Keywords AC electroosmotic flows · AC-EOF · In-plane microvortex · Pumping flow

1 Introduction

Recently, AC electroosmotic flow (AC-EOF) has attracted an increasing research interest, and shown great potential for lab-on-a-chip applications, such as fluid pumping (Brown et al. 2001; Debesset et al. 2004; Kuo and Liu 2008), fluid mixing (Sasaki et al. 2006; Kim et al. 2007), transportation (Tresset and Takeuchi 2005; Hilber et al. 2008), as well as concentration of bioparticles (Wong et al. 2004; Bown and Meinhart 2006), with its low-voltage operation (<10 V_{rms}), and operated frequency below 1 MHz. Basically, AC-induced flow originates from the applied AC voltage to planar electrodes immersed in a liquid electrolyte. The applied AC voltage induced the polarization of the electrode surface and the formation of a diffuse charged layer (or called as the electric double layer (EDL)) that serves to screen the external electric field applied. This type of electrode polarization is known as capacitive charging. Fluid movement is driven by the interaction between the tangential component of the electric field and the charges within the EDL. In our previous research (Huang et al. 2007), we demonstrated for the first time the patterned AC-EOF flow using various interdigitated electrode configurations to locally and simultaneously generate in-plane microvortices of clockwise, counter-clockwise, or pair rotation in a microchannel. By employing the microvortices, we also demonstrated the AC-EOF micromixer carried out for either rapid local

S.-H. Huang (✉) · H.-J. Hsueh
Department of Mechanical and Mechatronic Engineering,
National Taiwan Ocean University, No. 2, Beining Rd.,
Keelung 202-24, Taiwan, ROC
e-mail: shihhao@mail.ntou.edu.tw

K.-Y. Hung
Institute of Mechanical and Electrical Engineering,
Mingchi University of Technology, Taipei 243-01, Taiwan, ROC

mixing of two stationary fluids or continuous mixing of two flowing fluids. However, the rotational direction of in-plane microvortices predominately depends on the geometric asymmetry of the interdigitated electrode configurations, which cannot directly switch the clockwise and counter-clockwise microvortices using the same electrode configuration as shown in Fig. 1a.

To achieve this purpose, we need to have the ability to reverse the flow direction. Recently, the AC-EOF pumping flow has been shown to reverse the pumping direction at higher voltages and frequencies using the same electrode configuration (Studer et al. 2004; Olesen et al. 2006; Gregersen et al. 2007). Although theoretical models for pumping reversal have not been fully established, it has been suggested that the reason for the flow reversal is Faradaic charging or the injection of charges into the solution from the water electrolytic reactions at the electrode surface. The electrochemical reactions generate cations on the electrode surface, where the electrical charges

develop with a polarity of the same sign as that of the electrode. Thus, the flow direction driven by Faradaic charging is opposite to that driven by capacitive charging. Moreover, the undesirable effects associated with high voltages could cause the formation of bubbles due to electrolysis and the degradation of the electrodes. To overcome this problem, the asymmetric electrode polarization process was proposed to break the electrode symmetry (Wu 2008). A DC bias is superimposed onto AC potentials, so that the two electrodes in a pair undergo capacitive charging or Faradaic charging separately. By controlling capacitive and Faradaic charging, it enabled to reverse the flow direction using the same electrode configuration with only a few volts of applied voltages. Moreover, a numerical model for AC electroosmotic pumping was proposed to demonstrate the possibility to control the direction of the pumping velocity by grouping similar electrodes together, in order to create configurable asymmetries in periodic electrode arrays (Loucaides et al. 2007).

Here, we propose a configurable AC-EOF system based on capacitive charging by simply grouping discrete electrodes together to form various electrode configurations for generation of in-plane microvortices with clockwise, counter-clockwise rotation, and pumping flow in a microchannel. The rotational direction of in-plane microvortices and pumping flow direction can be controlled using the same electrode pattern by simple switching of the voltages on the electrodes. Microparticle image velocimetry (μ PIV) was used to characterize the flow fields of the generated in-plane microvortices and pumping flow. The rotational strength of the generated in-plane microvortices, flow rates of the pumping flow, and the performance discrepancy between the interdigitated and discrete electrode configurations were discussed in details in the following sections.

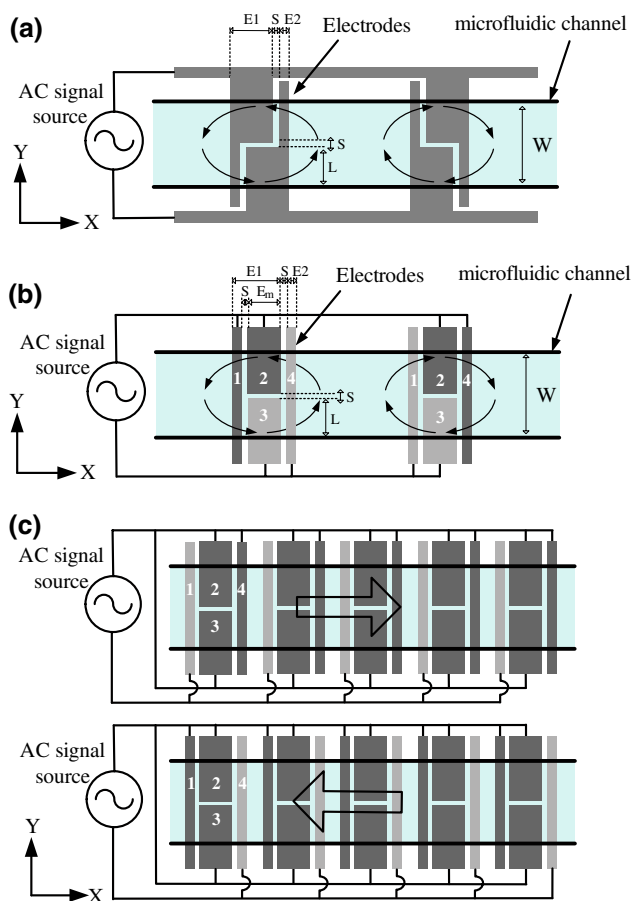


Fig. 1 Schematic diagrams of **a** the interdigitated, **b** the discrete electrode configurations for generation of in-plane microvortices with clockwise/counter-clockwise rotation, and **c** the configurable AC-EOF micropump with the discrete electrode configuration in a microchannel

2 Design concept

2.1 The configurable AC-EOF systems

Figure 1 shows the schematic diagrams of the interdigitated and discrete electrode configurations for generation of in-plane microvortices with clockwise/counter-clockwise rotation, and the configurable AC-EOF micropump with the discrete electrode configuration in a microchannel. Using the interdigitated electrode configuration, the local generation of in-plane microvortices with clockwise and counter-clockwise rotation has been successfully demonstrated in our previous research (Huang et al. 2007) as shown in Fig. 1a. The concept is derived from the micropump based on the AC-EOF principle. Briefly, the directional pumping of the whole fluid for AC-EOF micropump

is dependent on the geometric asymmetry of the electrodes, where a left-directed flow is produced for a series of paired electrodes with each small electrode located on the right side of the large electrode, and vice versa. To generate flow patterns with a local in-plane microvortex, we can reconfigure a pair of interdigitated electrodes with large and small electrodes arranged side by side in an opposite configuration, where the upper half and lower half of the paired electrodes can simultaneously produce flows in opposite directions. A locally in-plane microvortex with the clockwise/counter-clockwise rotation would then be realized. However, the rotational direction of in-plane microvortices predominately depends on the geometric asymmetry of the interdigitated electrode configuration, which cannot directly switch the clockwise and counter-clockwise microvortices using the same electrode configuration as shown in Fig. 1a and b.

Therefore, we proposed the configurable AC-EOF systems with the discrete electrode configuration for generation of in-plane microvortices with clockwise/counter-clockwise rotation, and pumping flow in a microchannel (Fig. 1b and c). The discrete electrode configuration is composed of two pairs of large and small electrodes. By applying the AC voltage on grouping electrode 1 and 2 with grouping electrode 3 and 4, the new electrode configuration (Fig. 1b, left) involves a pair of discrete electrodes in an opposite configuration similar to the interdigitated electrode configuration (Fig. 1a, left), where the upper half and lower half of the electrodes can simultaneously produce flows in opposite directions. An in-plane microvortex with the counter-clockwise rotation would then be realized. Similarly, by grouping electrode 1 and 3 with grouping electrode 2 and 4, a clockwise in-plane microvortex can be generated using the same electrode configuration (Fig. 1b, right). In addition, we also proposed a configurable AC-EOF micropump with an array of the discrete electrode configurations. By applying the AC voltage on grouping electrode 2, 3, and 4 with electrode 1, a series of the electrode configuration with each small electrode located on the left side of the large electrode (Fig. 1c, top), produces a right-directed flow. Similarly, by grouping electrode 1, 2 and 3 with electrode 4, a left-directed flow can be produced using the same electrode configuration (Fig. 1c, bottom). By utilizing the same electrode configuration while simply grouping discrete electrodes together to form various electrode configurations, we can directly switch the pumping flow direction and in-plane microvortices with clockwise and counter-clockwise rotation. The coordinate system shown in Fig. 1 indicates that X-, Y- and Z-axis are the streamwise, spanwise, and cross-stream coordinates. The origin of the coordinate system is located at the centerline of the microchannel on the substrate surface. The X, Y components of the velocity are represented by U and V, respectively.

2.2 Performance analysis

According to the AC-EOF principle, the fluid flow of the AC-EOF micropump is sensitive to the applied frequency and voltage (Brown et al. 2001). It has been shown that velocity profiles for AC-EOF have an optimal value at an appropriately applied characteristic frequency f_0 expressed by Eq. 1

$$f_0 = \frac{\lambda_D \sigma}{\epsilon \pi^2 \sqrt{x_{\min} x_{\max}}} \tag{1}$$

where ϵ and σ are, respectively, permittivity and conductivity of the solution, and λ_D is the thickness of the double layer. x_{\min} and x_{\max} are the characteristic lengths for the electrode configuration. x_{\min} is equal to $S/(\sqrt{k} + 1/\sqrt{k})$, and x_{\max} is equal to $(S + E1 + E2)/(\sqrt{k} + 1/\sqrt{k})$. $E1$ and $E2$ denote the widths of the large and small electrodes, respectively, and S is the gap between them. k represents $E1/E2$, which is the ratio of the electrode widths. By means of the characteristic lengths measuring from an origin, a conduction path that starts at a distance of $x\sqrt{k}$ from this origin over the large electrode will end at a point x/\sqrt{k} from this origin over the small electrode (Brown et al. 2001) as shown in Fig. 2. At the characteristic frequency f_0 that gives a maximum velocity, the theoretical average velocity (v_{ave}) on the surface of the large electrodes is found to be

$$v_{ave} = \frac{\int_{x_{\min}}^{x_{\max}} <v_D(x)> dx}{x_{\max} - x_{\min}} = \frac{\Psi^2 v_0}{2(x_{\max} + x_{\min})} \tag{2}$$

where

$$v_0 = \frac{\epsilon}{2\mu\sqrt{k}(1+k)^2} \tag{3}$$

Ψ and μ represent the applied potential and the viscosity of the solution, respectively.

For the interdigitated electrode configuration, it consists of a large electrode of width ($E1$), separated from a small electrode of width ($E2$) by a small gap (S) (Fig. 2, top). For the discrete electrode configuration, it consists of a large electrode of width (Em), located at the middle of two small electrodes of width ($E2$) separated by a small gap (S), respectively (Fig. 2, bottom). The width (Em) of the large electrode is equal to the $E1-E2-S$. To compare the performance discrepancy, we set the $E1 = 100 \mu\text{m}$, $E2 = 20 \mu\text{m}$, $k = 5$, and $S = 20 \mu\text{m}$ for both the interdigitated and discrete electrode configurations. The characteristic lengths of x_{\min} , x_a , x_b , and x_{\max} are then calculated as 7.5, 42.1, 47.5, and 52.2 μm , respectively. According to Eq. 2, at the characteristic frequency f_0 , the theoretical percentage difference (η) of the average velocity (v_{ave}) on the electrode surfaces between the interdigitated and discrete electrode configurations is expressed as:

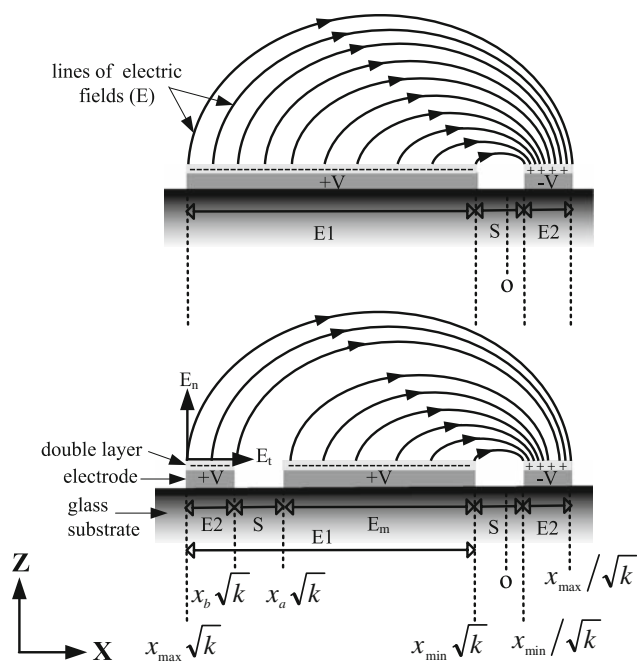


Fig. 2 The electric fields and characteristic lengths of the interdigitated and discrete electrode configurations in water at the instant that the large electrode is at a positive potential and the small electrode is at a negative potential (IEC and DEC indicate the interdigitated electrode configuration and discrete electrode configuration, respectively)

$$\eta(\%) = \frac{\int_{x_a}^{x_b} \langle v_D(x) \rangle dx}{\int_{x_{\min}}^{x_{\max}} \langle v_D(x) \rangle dx} \times 100\% = \frac{(x_{\max} + x_{\min})(x_a - x_b)}{(x_{\max} - x_{\min})(x_a + x_b)} \times 100\% \tag{4}$$

The theoretical percentage difference ($\eta(\%)$) of the average velocity (v_{ave}) is then calculated about 8% on the surface of the large electrodes in this case. This performance reduction of the average velocity for the discrete electrode configuration is derived from the decrease of the active electrode area. Besides, taking $\lambda_D = 100 \times 10^{-9}$ m, $\sigma = 0.003 \Omega^{-1} \text{ m}^{-1}$, and $\epsilon = 7.08 \times 10^{-8} \text{ F m}^{-1}$ for DI water (Lee et al. 2006) as the working liquid into Eq. 1, we obtained the theoretical resonant frequencies to be 2.17 kHz.

3 Experimental

The chips for generating AC-EOF were fabricated on a 1-mm thick glass substrate. A 200-nm thick gold layer with a 20-nm thick chromium adhesion layer was evaporated on the glass substrate. The electrode patterns were fabricated through photolithography and patterned by a wet etching process. The microfluidic channels of 5 cm length, $W = 600 \mu\text{m}$ width, and $H = 200 \mu\text{m}$ depth were made

of polydimethylsiloxane (PDMS, Dow Corning, USA) by using standard soft-lithography technique and precisely bonded onto the electrode substrate after oxygen plasma treatment. AC signals were provided by a function generator (Lecroy, LW120, USA) to the electrodes. Figure 3a–c shows the images of the interdigitated and the discrete electrode configurations as well as the configurable AC-EOF micropump with an array of the discrete electrode configuration, respectively. The configurable AC-EOF micropump was designed with 100 subunits of the discrete electrode configuration. The gap and pitch among the subunits were 60 and 400 μm , respectively. The velocity of the pumping flow and in-plane microvortices can be controlled by the applied voltages, frequencies and the electrode configurations.

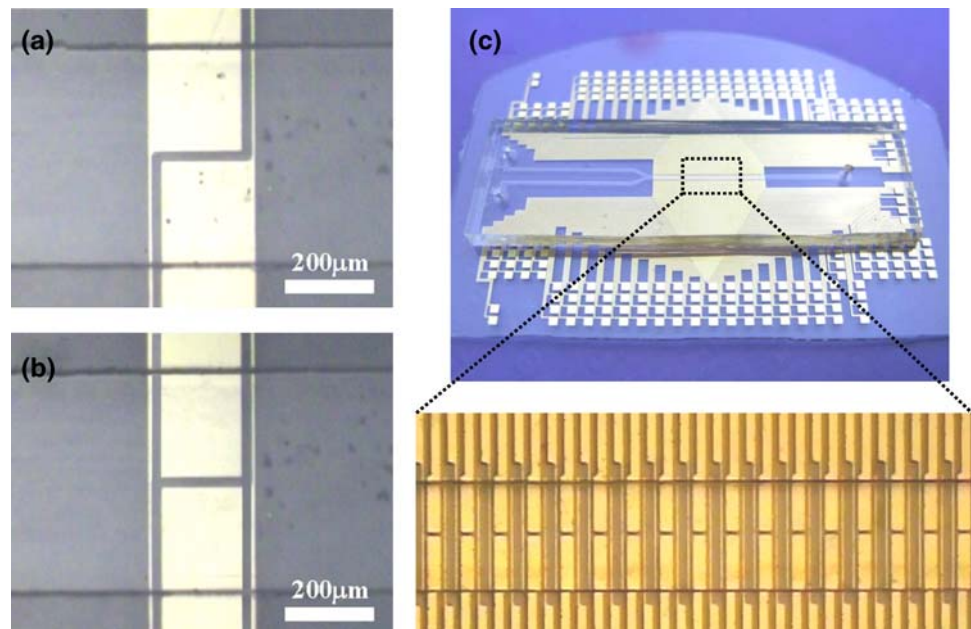
Microparticle image velocimetry (μPIV) was used to characterize the flow fields of the pumping flow and the in-plane microvortices. For further information regarding the setup of the μPIV technique used here, one might refer to our previous literature (Huang et al. 2007). Briefly, the in-plane microvortex patterns were observed at the X-Y planes with different channel heights ($Z = 20\text{--}180 \mu\text{m}$) by an adjustable optical stage with resolution of 1 μm , and the fluid velocities were measured by μPIV technique. This technique measures fluid motion by measuring the motion of fluorescent tracing particles suspended in a working fluid. The AC-EOF system was first operated at the applied voltage and frequency for lasting at least 30 min to stabilize the flow fields. The fluorescent particle images were then recorded using an epi-fluorescence microscope with the high-speed CCD. Polystyrene fluorescent-tagged particles, 1 μm in diameter at a volumetric density of 0.4% were used in the experiment. The images were analyzed using a cross correlation-based PIV software (TSI, Insight, USA) to obtain velocity-vector fields, and averaging of the ten data sets for each measurement to minimize variation in velocity fields. The coefficient of variation (CV) of the data calculated from the velocity fields for five different tests in each the applied voltage and frequency was smaller than 5%. The result shows the convincing reproducibility of the current AC-EOF system. The CV is defined as the ratio of the standard deviation to the mean value.

4 Results and discussions

4.1 Characteristics of in-plane microvortices and pumping flow

Figure 4a–c shows the velocity fields of in-plane microvortex with clockwise/counter-clockwise rotation, and pumping flow for the discrete electrode configuration measured at the middle plane ($Z = 100 \mu\text{m}$) of the

Fig. 3 Images of **a** the interdigitated and **b** the discrete electrode configurations, and **c** the configurable AC-EOF micropump with an array of one hundred subunits of the discrete electrode configuration



microchannel using the μ PIV technique under $V_{p-p} = 16$ V at 2 kHz. By applying the AC voltage on grouping electrode 1 and 3 with grouping electrode 2 and 4, we successfully demonstrated the in-plane microvortex with the clockwise rotation (Fig. 4a). We clearly observed the microsphere tracer rotating clockwise in the depth of focus of the observation system at the middle plane ($Z = 100$ μ m). Similarly, we can also demonstrate the in-plane microvortex with the counter-clockwise rotation (Fig. 4b). By utilizing the same electrode configuration while simply grouping discrete electrodes together to form various electrode configurations, we can directly switch in-plane microvortices with clockwise and counter-clockwise rotation. We also observed the in-plane microvortices at the different heights of the measured X - Y planes ranging from $Z = 20$ to 180 μ m during the velocity field measurement. Because the electrode configuration was only fabricated at the bottom of the microchannel ($Z = 0$ μ m), the rotational strength of in-plane microvortices decreased as increasing the heights of the measured planes from $Z = 20$ –180 μ m. However, we could hardly see the complete structure of in-plane microvortices below $Z = 40$ μ m. Instead, we observed the small out-of-plane vortices above the small electrodes near electrode surfaces. The small out-of-plane vortices deformed the structure of in-plane microvortices. The size of the vortices was in the same order of the magnitude as the width of the small electrodes. In addition, by applying the AC voltage on grouping electrode 2, 3, and 4 with electrode 1, we demonstrated the possibility for generation of the pumping flow. Figure 4c shows the velocity field of a right-directed flow using one unit of the discrete electrode configuration.

The right-directed flow was successfully produced via grouping electrode 2, 3, and 4 with electrode 1, where the small electrode is located on the left side of the large electrode. Accordingly, by extending one unit into an array of 100 subunits of the discrete electrode configuration, a right-directed pumping flow can be produced in the microchannel.

To characterize the generated in-plane microvortices using the discrete electrode configuration, we measured the transverse velocity $V(x)$ along the centerlines of microchannel across the clockwise microvortices operated at applied voltages of $V_{p-p} = 8$ –20 V and at 2 kHz, and counter-clockwise microvortices operated at $V_{p-p} = 16$ V and at 2 kHz, respectively (Fig. 5). All velocity profiles were plotted together by defining the origin of X -axis coordinate in Fig. 5 to be at the vortex core, where $V(x)$ was approximately equal to 0. The velocity profiles show typical viscous microvortices, antisymmetric with respect to the centerline of the microvortex. The magnitudes of $V(x)$ start to increase, reach maximum values, and decrease to zero as they approach to the vortex core. For the clockwise and counter-clockwise microvortices both operated at $V_{p-p} = 16$ V and at 2 kHz, the distribution of transverse velocity $V(x)$ shows the same tendency and maximum values, but in the opposite direction. It indicates that the rotational direction of the generated in-plane microvortices can be controlled by simple switching of the voltages on the electrodes without influence of the flow patterns.

To quantitatively characterize the active region size and the rotational strength of the microvortex, we define the length (D_{active}) of the active region and the magnitude (Ω) of the rotational strength as

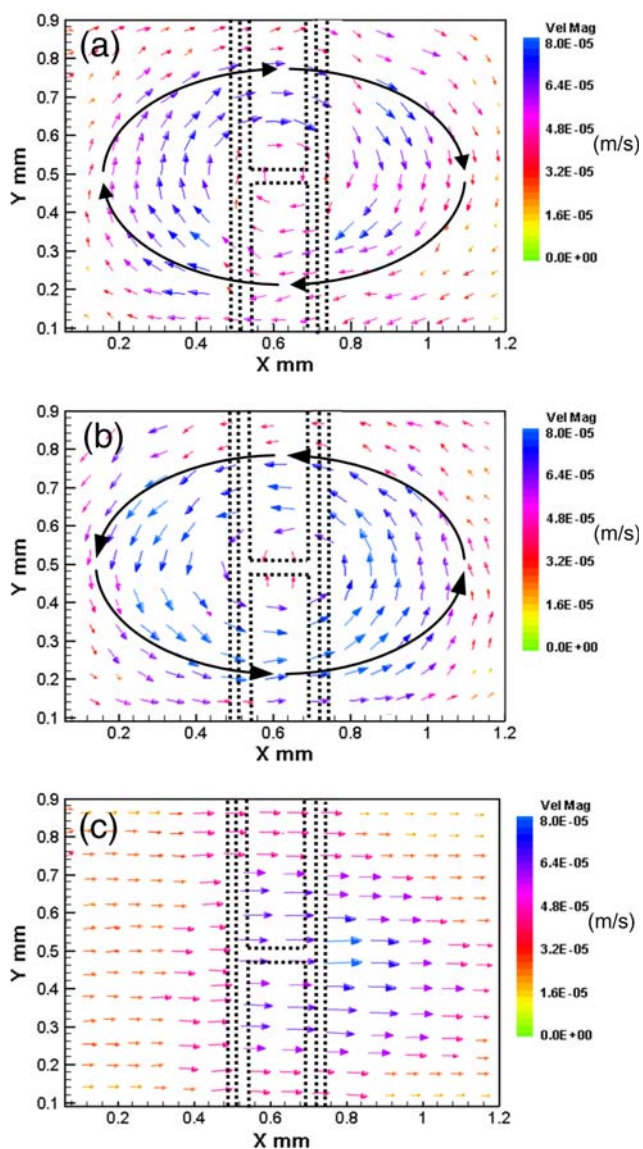


Fig. 4 Velocity fields of **a** the in-plane microvortex with clockwise, and **b** counter-clockwise rotation, and **c** pumping flow for the discrete electrode configuration measured at the middle plane ($Z = 100 \mu\text{m}$) of the microchannel using the μPIV technique under $V_{\text{p-p}} = 16 \text{ V}$ at 2 kHz

$$D_{\text{active}} = |D_R| + |D_L| \quad (6)$$

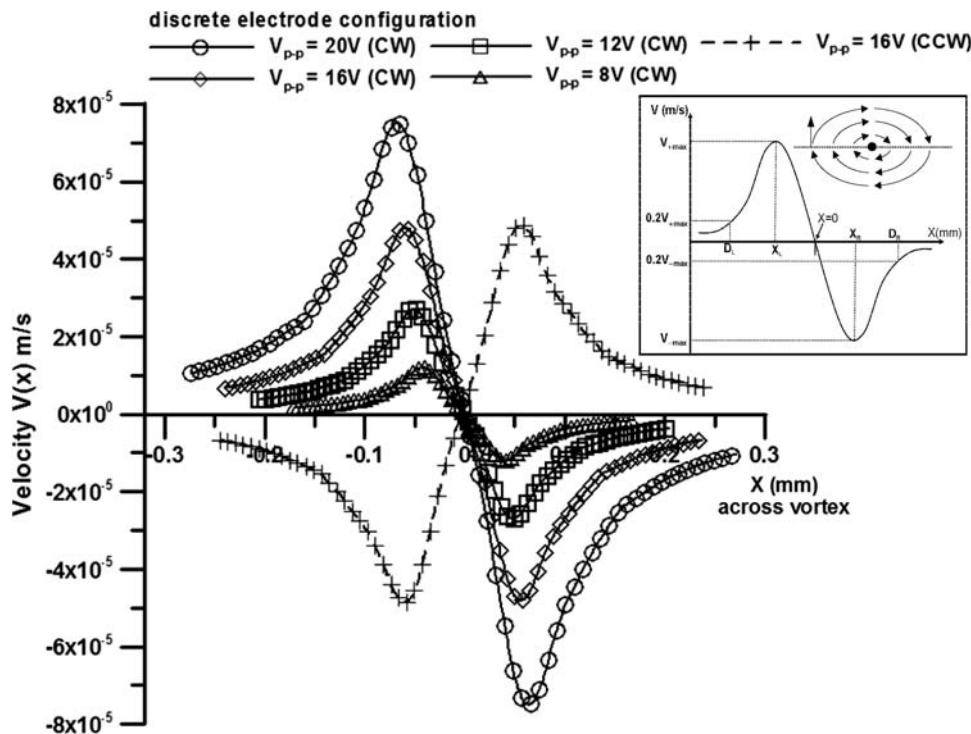
$$\Omega = \frac{|V_{+\text{max}}| + |V_{-\text{max}}|}{|X_R| + |X_L|} \quad (7)$$

where D_R and D_L denote the distances as $V(x)$ decreases to the 20% magnitudes of the maximum velocities ($V_{+\text{max}}$ and $V_{-\text{max}}$), as illustrated in the inset of Fig. 5. X_R and X_L denote the distances where $V(x)$ reaches at the maximum values ($V_{+\text{max}}$ and $V_{-\text{max}}$). As can be seen, the magnitudes of the maximum velocity (V_{max}) increase with the increase in the applied voltages at $V_{\text{p-p}} = 8\text{--}20 \text{ V}$. The increase in the maximum velocity results in the increase of the active

region size (D_{active}) indicating an expansion of the in-plane microvortices with higher applied voltages. For instance, $V_{+\text{max}}$ and D_{active} are $27 \mu\text{m/s}$ and 0.32 mm for $V_{\text{p-p}} = 12 \text{ V}$, while $76 \mu\text{m/s}$ and 0.46 mm for $V_{\text{p-p}} = 20 \text{ V}$. Increasing the applied voltages can lead to the expansion and increase of the rotational strength of the in-plane microvortices.

Figure 6 shows the voltage dependence of the rotational strength (Ω) for in-plane microvortices and maximum velocity (U) for pumping flow with an array of 100 subunits of the discrete electrode configuration at 2 kHz . Increasing the applied voltages can lead to the increase of the rotational strength of the in-plane microvortices and the maximum velocity for pumping flow. Both the rotational strength (Ω) and maximum velocity show the same tendency of the voltage dependence. The tendency corresponds to the flow velocities on the electrode surface, which vary proportional with the square of the applied voltages (shown in Eq. 2). Although the flow velocities of the in-plane microvortices and pumping flow can be adjusted by changing the applied voltages, we found that it needed more than 10 min to stabilize the flow velocity due to the inertial force after decreasing or increasing the applied voltages. At a lower applied voltage of $V_{\text{p-p}} = 4 \text{ V}$, the rotational strength (Ω) of the in-plane microvortex decreased to a smaller value of 0.1 s^{-1} at the middle plane ($H = 100 \mu\text{m}$) of the microchannel. A very weak rotation of the in-plane microvortex was observed at $V_{\text{p-p}} = 4 \text{ V}$. It indicates that the penetration depth of the surface force originated from AC-EOF was about $100 \mu\text{m}$. Hardly, can we measure or observe the in-plane microvortex at an applied voltage below $V_{\text{p-p}} = 4 \text{ V}$ in the middle plane ($H = 100 \mu\text{m}$) of the microchannel. At a higher applied voltage of $V_{\text{p-p}} = 20 \text{ V}$, a stronger rotation of the in-plane microvortex and faster velocity of the pumping flow were observed to last at least 30 min without generation of gas bubbles and electrodes degradation. It is to be noted that most of the AC-EOF micropumps reported in the literatures encountered the problem of gas bubbles at $V_{\text{p-p}} = 20 \text{ V}$. It is attributed to the fact that the relatively larger gap of $20 \mu\text{m}$ between the applied electrodes, larger electrode width of $100 \mu\text{m}$, and DI water used in our experiments increased the threshold of the applied voltages for occurrence of electrolysis. At an applied voltage higher than $V_{\text{p-p}} = 20 \text{ V}$, the electrodes degraded and air bubbles generated because of unavoidable heating and electrochemical reactions in the fluid. Future improvement of the device should aim at reducing electrode erosion, for example using new electrode materials such as ITO (indium tin oxide) or to cover the electrodes by using a dielectric protection film.

Fig. 5 The transverse velocity $V(x)$ along the centerlines of microchannel across the clockwise microvortices operated at applied voltages of $V_{p-p} = 8\text{--}20$ V and at 2 kHz, and counter-clockwise microvortices operated at $V_{p-p} = 16$ V and at 2 kHz, respectively (CW clockwise rotation, CCW counter-clockwise rotation)



4.2 Performance discrepancy of the interdigitated and discrete electrode configurations

Figure 7a shows the frequency dependence on the rotational strength (Ω) of in-plane microvortices and percentage difference ($\delta(\%)$) of the rotational strength between the interdigitated and discrete electrode configurations. The percentage difference ($\delta(\%)$) is calculated by $(\Omega^* - \Omega) / \Omega^* \times 100\%$, where Ω^* and Ω represent the rotational strength of in-plane microvortices for the interdigitated and discrete electrode configurations, respectively. At fixed voltage ($V_{p-p} = 16$ V) while changing operated frequency from 700 to 3.5 kHz, we found that the rotational strength for in-plane microvortices reached a maximum value at a frequency about 2 kHz for both the interdigitated and discrete electrode configurations. The optimal rotational strength at 2 kHz is approximately consistent with the theoretical resonant frequencies to be 2.17 kHz. Note that the discrepancy in electrode geometry between the interdigitated and discrete electrode configuration did not significantly change the characteristic frequency. This is due to the fact that the characteristic frequency (f_0) in Eq. 1 is directly related to the characteristic lengths of x_{min} , x_{max} , and $k = E1/E2$, which are of the same values for both the interdigitated and discrete electrode configurations in this case. However, it seems to influence the magnitudes of the rotational strength of in-plane microvortices at the given applied voltage. The percentage difference ($\delta(\%)$) of the rotational strength was found to have a maximum value of

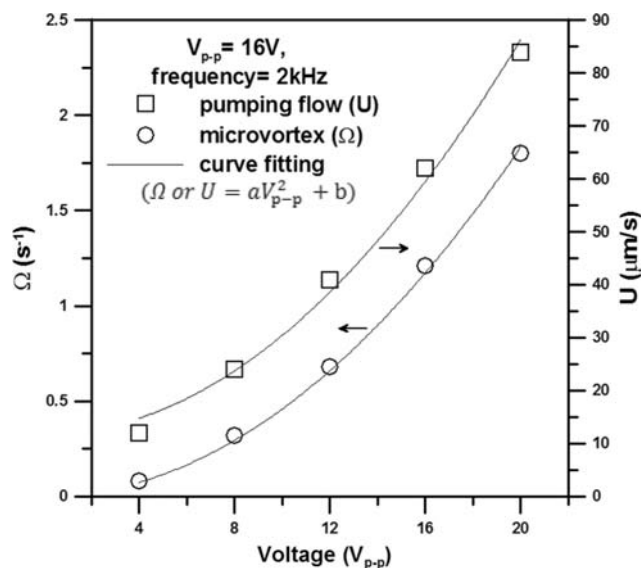


Fig. 6 The voltage dependence of the rotational strength (Ω) for in-plane microvortices and maximum velocity (U) for pumping flow with an array of one hundred subunits of the discrete electrode configuration at the middle plane ($Z = 100 \mu\text{m}$) of the microchannel and at 2 kHz (The fitted curves: Ω or $U = aV_{p-p}^2 + b$, where a and b are constants)

30% at the characteristic frequency of 2 kHz. At low frequencies, the majority of the electric potential drop occurs across the EDL. The tangential component of the electric field is at a minimum stage at these frequencies. Therefore, the percentage difference ($\delta(\%)$) of the rotational strength

decreased due to the significant decrease of AC-EOF velocities for both the interdigitated and discrete electrode configurations. At high frequencies, the net charge in the EDL does not respond accordingly. The significant decrease in AC-EOF velocities leads to the decrease of the percentage difference ($\delta(\%)$) of the rotational strength at high frequencies. It indicates that the discrepancy in electrode geometry did not have a significant contribution to the AC-EOF velocities at both low and high frequencies. Although the percentage difference ($\delta(\%)$) has a maximum value of 30% at the characteristic frequency of 2 kHz, this is lower for other frequency. This performance reduction can be more than compensated for being able to produce configurable flow patterns using the same electrode configuration. The percentage difference ($\delta(\%)$) of the rotational strength has a maximum value at the characteristic frequency, which is consistently in agreement with the previous literature in Loucaides et al. (2007). They used a numerical model to indicate the same trend for a configurable AC electroosmotic pumping by grouping similar electrodes together.

Figure 7b shows the voltage dependence on the rotational strength (Ω) of in-plane microvortices and percentage difference ($\delta(\%)$) of the rotational strength between the interdigitated and discrete electrode configurations. It can be seen, for all the applied voltages, the rotational strength of in-plane microvortices for the interdigitated electrode configuration is larger than that of the discrete electrode configuration. The percentage difference ($\delta(\%)$) of the rotational strength shows a constant value about 30% as increasing the applied voltages from $V_{p-p} = 12$ to 20 V. The result indicates that no matter what the voltages were applied, the discrepancy in electrode geometry led to the performance reduction around 30% between the interdigitated and discrete electrode configurations at 2 kHz and at the middle plane of the channel in this case. Changing the operated frequency to low or high frequencies can result in the decrease of the percentage difference ($\delta(\%)$) as shown in Fig. 7a. In addition, decreasing the discrepancy in electrode geometry can also lead to the decrease of the percentage difference ($\delta(\%)$). However, according to Eq. 4, the theoretical percentage difference ($\eta(\%)$) of the average velocity (v_{ave}) on electrode surfaces is 8%, which is significantly smaller than 30% for the reduction of the rotational strength measured at the middle plane of the microchannel.

To examine the height effect of the measured X-Y planes, we measured the rotational strength of in-plane microvortices at the X-Y planes with different channel heights ($Z = 40$ – $180 \mu\text{m}$) as shown in Fig. 7c. The result

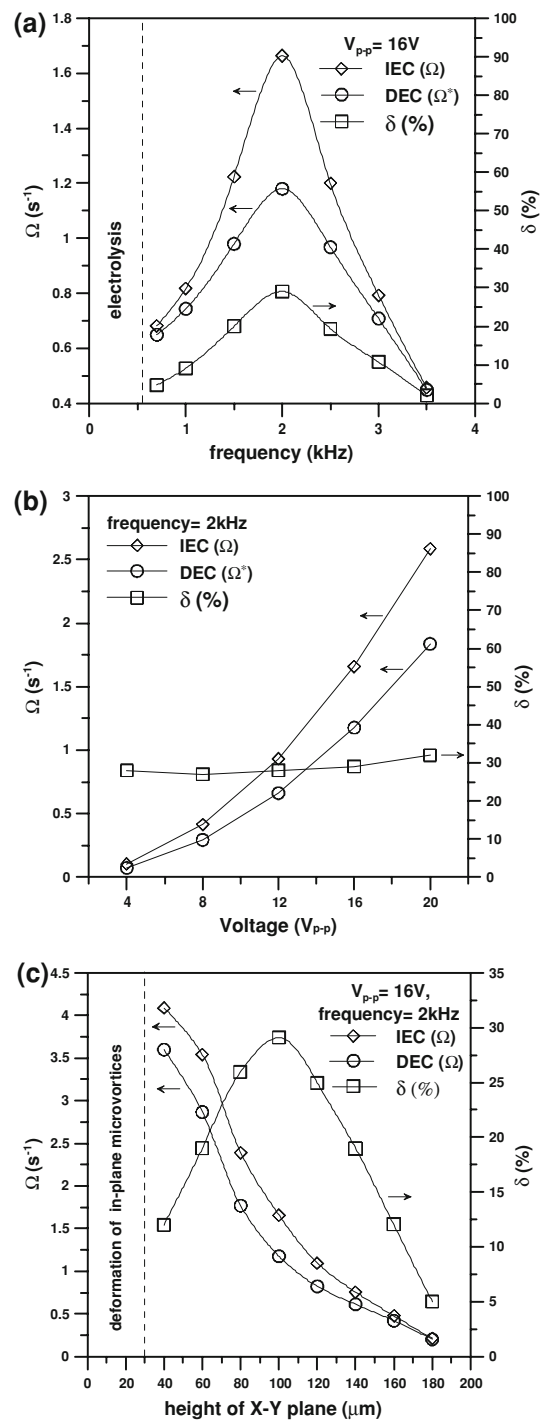


Fig. 7 Dependence of **a** the applied voltage, **b** the operated frequency at the middle plane ($Z = 100 \mu\text{m}$), and **c** the height of the measured X-Y planes on the rotational strength of in-plane microvortices, and percentage difference ($\delta(\%)$) of the rotational strength for the interdigitated and discrete electrode configurations (IEC and DEC indicate the interdigitated electrode configuration and discrete electrode configuration, respectively)

shows that the rotational strength (Ω) of in-plane microvortices for the interdigitated and discrete electrode configurations decreased with increasing heights of the measured X - Y planes. This is due to the fact that the applied electrodes were only located at the bottom of the substrate. Figure 7c also shows the height dependence of the percentage difference ($\delta(\%)$) of the rotational strength between the interdigitated and discrete electrode configurations. The percentage difference ($\delta(\%)$) was found to have a maximum 30% at the middle plane ($Z = 100 \mu\text{m}$) of the microchannel. As decreasing the height of the measured planes to be at $Z = 40 \mu\text{m}$ near the applied electrode surfaces, the performance reduction of the rotational strength is about 13%, which is close to the theoretical percentage difference ($\eta(\%)$) of the average velocity (v_{ave}) about 8% on the electrode surfaces. It indicates that the decrease of the height of the X - Y planes near the applied electrode surfaces can decrease the percentage difference ($\delta(\%)$) between the interdigitated and discrete electrode configurations due to the discrepancy in electrode geometry. With the increasing height of the X - Y planes from $Z = 100$ to $180 \mu\text{m}$, the percentage difference ($\delta(\%)$) decreased due to no slip condition on the channel surface, where the velocity significantly decreased for both interdigitated and discrete electrode configurations.

5 Conclusion

We proposed a novel design concept of the configurable AC-EOF systems by simply grouping discrete electrodes together to form various electrode configurations for generation of in-plane microvortices with clockwise/counter-clockwise rotation, and pumping flow in a microchannel. The rotational direction of in-plane microvortices and pumping flow direction can be controlled using the same electrode pattern by simple switching of the voltages on the electrodes. Although a performance reduction between the interdigitated and discrete electrode configurations existed, this can be reduced by the decrease of the discrepancy in electrode geometry. This small performance reduction can be more than compensated by the ability of switching the pumping flow direction or the rotational direction of in-plane microvortices using the same device. Moreover, by employing the configurable in-plane microvortices and pumping flow, the AC-EOF micromixer can be used for continuous mixing of two flowing fluids for micro mixing

applications. Simple fabrication and easy operation also provide the potential for the integration into a lab-on-a-chip system.

Acknowledgments This work was partially supported by National Science Council, Taiwan, through the grant NSC 97-2218-E-019-001-MY2.

References

- Bown MR, Meinhart CD (2006) AC electroosmotic flow in a DNA concentrator. *J Microfluid Nanofluid* 2(6):513–523
- Brown ABD, Smith CG, Rennie AR (2001) Pumping of water with ac electric fields applied to asymmetric pairs of microelectrodes. *Phys Rev E* 63:016305
- Debesset S, Hayden CJ, Dalton C, Eijkel JC, Manz A (2004) An AC electroosmotic micropump for circular chromatographic applications. *Lab Chip* 4:396–400
- Gregersen M, Olesen L, Brask A, Hansen M, Bruus H (2007) Flow reversal at low voltage and low frequency in a microfabricated ac electrokinetic pump. *Phys Rev E* 76:056305
- Hilber W, Weiss B, Mikolasek M, Holly R, Hingerl K, Jakoby B (2008) Particle manipulation using 3D ac electro-osmotic micropumps. *J Micromech Microeng* 18(6):064016
- Huang SH, Wang SK, Khoo HS, Tseng FG (2007) AC electroosmotic generated in-plane microvortices for stationary or continuous fluid mixing. *Sens Actuator B* 125(1):326–336
- Kim BJ, Yoon SY, Sung HJ, Smith CG (2007) Simultaneous mixing and pumping using asymmetric microelectrodes. *J Appl Phys* 102(7):074513
- Kuo CT, Liu CH (2008) A novel microfluidic driver via AC electrokinetics. *Lab Chip* 8(5):725–733
- Lee ML, Hau WLW, Lee YK, Zohar Y (2006) In-plane vortex flow in microchannels generated by electroosmosis with patterned surface charge. *J Micromech Microeng* 16:17–26
- Loucaides N, Ramos A, Georghiou GE (2007) Novel systems for configurable AC electroosmotic pumping. *J Microfluid Nanofluid* 3(6):709–714
- Olesen L, Bruus H, Ajdari A (2006) Ac electrokinetic micropumps: the effect of geometrical confinement, faradaic current injection, and nonlinear surface capacitance. *Phys Rev E* 73(5):056313
- Sasaki N, Kitamori T, Kim HB (2006) AC electroosmotic micromixer for chemical processing in a microchannel. *Lab Chip* 6:550–554
- Studer V, Pe'pin A, Chen Y, Ajdari A (2004) An integrated ac electrokinetic pump in a microfluidic loop for fast and tunable flow control. *Analyst* 129:944–949
- Tresset G, Takeuchi S (2005) Utilization of cell-sized lipid containers for nanostructure and macromolecule handling in microfabricated devices. *Anal Chem* 77:2795–2801
- Wong PK, Chen CY, Wang TH, Ho CM (2004) Electrokinetic bioprocessor for concentrating cells and molecules. *Anal Chem* 76:6908–6914
- Wu J (2008) Ac electro-osmotic micropump by asymmetric electrode polarization. *J Appl Phys* 103(2):024907